


Article

# Incorporation of Amino Acid-Functionalized Ionic Liquids into Highly Porous MOF-177 to Improve the Post-Combustion CO<sub>2</sub> Capture Capacity

Firuz A. Philip and Amr Henni \* 

Faculty of Engineering and Applied Science, University of Regina, Regina, SK S4S 0A2, Canada; philip2f@uregina.ca

\* Correspondence: amr.henni@uregina.ca

**Abstract:** This study presents the encapsulation of two amino acid-based ionic liquids (AILs), 1-ethyl-3-methylimidazolium glycine [Emim][Gly] and 1-ethyl-3-methylimidazolium alanine [Emim][Ala], in a highly porous metal–organic framework (MOF-177) to generate state-of-the-art composites for post-combustion CO<sub>2</sub> capture. Thermogravimetric analysis (TGA) demonstrated a successful encapsulation of the AILs, with a dramatic reduction in the composites' surface areas and pore volumes. Both [Emim][Gly]@MOF-177 and [Emim][Ala]@MOF-177 had close to three times the CO<sub>2</sub> uptake of MOF-177 at 20 wt.% loading, 0.2 bar, and 303 K. Additionally, 20-[Emim][Gly]@MOF-177 and 20-[Emim][Ala]@MOF-177 enhanced their CO<sub>2</sub>/N<sub>2</sub> selectivity from 5 (pristine MOF-177) to 13 and 11, respectively.

**Keywords:** CO<sub>2</sub> capture; metal organic framework (MOF); ionic liquid; amino acid ionic liquid (AIL); task-specific ionic liquid (TSIL); MOF-177



**Citation:** Philip, F.A.; Henni, A. Incorporation of Amino Acid-Functionalized Ionic Liquids into Highly Porous MOF-177 to Improve the Post-Combustion CO<sub>2</sub> Capture Capacity. *Molecules* **2023**, *28*, 7185. <https://doi.org/10.3390/molecules28207185>

Academic Editors: Rui Li, Yi Lu and Zhehui Jin

Received: 15 September 2023

Revised: 12 October 2023

Accepted: 17 October 2023

Published: 20 October 2023



**Copyright:** © 2023 by the authors. Licensee MDPI, Basel, Switzerland. This article is an open access article distributed under the terms and conditions of the Creative Commons Attribution (CC BY) license (<https://creativecommons.org/licenses/by/4.0/>).

## 1. Introduction

Metal–organic-frameworks, often known as MOFs, are a unique class of porous materials that are currently the subject of substantial research for a broad variety of applications [1,2], notably, the storage and separation of gases, catalysis, the delivery of drugs, and energy storage [3–8]. MOFs are typically three-dimensional structures that have high surface area and porosity. These structures are formed from metal nodes that are coupled with organic linkers. MOFs have lately gained an enormous amount of popularity for applications in CO<sub>2</sub> capture and storage because of their high porosity as well as their great potential for gas capture or storage due to their tunability [2,9–12]. Although some MOFs have displayed superb absorbance of CO<sub>2</sub> at high pressure, in post-combustion conditions, in which the partial pressure of CO<sub>2</sub> is in general about or lower than 0.15 bar, they showed very low CO<sub>2</sub> uptake [13]. To enhance their CO<sub>2</sub> capture capability, many strategies have been deployed including the introduction of open metal sites [14], the covalent grafting of amine functionalities to the ligands [15–17], the impregnation of amines [18–21], and the addition of ionic liquids (ILs) [22]. The physical impregnation of amines led to a higher CO<sub>2</sub> uptake compared to the covalent grafting of amines, as a higher amine loading could be achieved by impregnation. Nonetheless, amine-impregnated sorbents are susceptible to amine loss and degradation and require a high regeneration energy [13]. Ionic liquids (ILs) have been proposed as an attractive alternative to amines partly due to their low volatility and high thermal stability; however, it was reported that in some cases, the CO<sub>2</sub> uptake rather diminished for IL-modified sorbents, although improved selectivity was observed [23–25].

The first amine-functionalized ionic liquids (AILs) were developed by Bates et al. [26], demonstrating that the CO<sub>2</sub> sorption capacity of ILs can be substantially enhanced by functionalizing the sorbent with amine groups (-NH<sub>2</sub>) while at the same time retaining ILs'

properties. Since then, numerous AILs, referred to as task-specific ionic liquids (TSILs), have been reported in the scientific literature. Among them, amino acid anion-functionalized ionic liquids (AAILs) have the clear advantages of an easy synthesis process, a low cost, biodegradability, and the requirement of environmentally friendly raw materials, as they are sourced from naturally occurring amino acids (AAs) [27–29]. As a result, AAILs are deemed promising candidates to functionalize porous MOFs and lead to advanced sorbents with high CO<sub>2</sub> capture capacity. Several researchers demonstrated that the immobilization of AAILs into solid sorbents such as MCM-41, SBA-15, and PMMA led to an increase in carbon dioxide adsorption [30–33].

Recently, we showed that AAILs containing reactive amino acid (AA) anions such as glycine [Gly] and alanine [Ala] acted as effective guest molecules in a solid ZIF-8 support, significantly increasing CO<sub>2</sub> uptake and CO<sub>2</sub>/N<sub>2</sub> selectivity [34]. Hence, we aimed to expand our study and investigate new composites by impregnating these AAILs into MOF-177 as a host sorbent, which is one of the highest porous MOFs reported to date, with a pore volume of 1.69 cm<sup>3</sup>/g and a BET-specific surface area of over 4000 m<sup>2</sup>/g [35,36]. MOF-177 displays a 3D crystalline framework consisting of zinc metal clusters and 1, 3, 5-benzene tribenzoate (BTB) organic linkers. Owing to its high porosity and volume, it displayed an outstanding CO<sub>2</sub> uptake performance (60.8 wt.%) at high pressure (50 bar); however, the CO<sub>2</sub> uptake at low pressure (0.15 bar) was very poor (0.6 wt.%) [13]. This led us to embark on this study and incorporate AAILs into highly porous MOF-177, obtaining AAILs@MOF-177 composites with improved active sorption sites, anticipating that this strategy would lead to a higher potential for CO<sub>2</sub> capture in post-combustion conditions. We are unaware of any published prior work involving these composites. In this study, we investigated the composites and compared them to pure MOF-177 in terms of thermal stability, crystal structure, and textural qualities. The produced composites' potentials in real-world CO<sub>2</sub> capture operations were investigated by examining their CO<sub>2</sub> capture capacity, selectivity, and enthalpy of adsorption.

## 2. Results and Discussion

### 2.1. Characterization of the AAIL-Impregnated Sorbents

A thermogravimetric analysis of MOF-177 and the AAILs@MOF-177 composites was performed to monitor the thermal stability of the AAIL-supported MOF-177 composites from 25 to 800 °C in a nitrogen atmosphere. TGA thermograms of the composites along with those of pure AAILs and pristine MOF-177 are presented in Figure 1a–d. The thermograms of pristine [Emim][Gly] and [Emim][Ala] indicated that both AAILs were thermally stable up to 200 °C, but beyond that temperature, a sharp weight loss was observed, indicating a very rapid decomposition. According to the derivative weight loss profile shown in Figure 1b,d, it was found that the onset decomposition temperatures ( $T_{\text{onset}}$ ) were about 215 °C and 225 °C, respectively, whereas the pristine solid support MOF-177 was much more thermally stable than the pristine AAILs, with onset decomposition temperatures ( $T_{\text{onset}}$ ) of about 421 °C, in agreement with similar studies reported in the literature [36,37]. A little decrease in weight of around 2 to 4 wt.% was found for the composites at temperatures under 75 °C. This drop can most probably be attributed to the potential evaporation of any residual methanol (BP of 65 °C) that was employed during the synthesis of the composites. The thermogram of the composites revealed that the incorporated AAILs decomposed before the pristine solid support itself, as expected. However, note that there was no sharp decomposition of AAILs around their  $T_{\text{onset}}$ , but rather, a gradual decomposition over the temperature range from 250 to 400 °C, which continued until MOF-177 itself started to decompose, as displayed in Figure 1b,d. This gradual decomposition was more profound at higher loadings of AAILs, as observed for 30-[Emim][Gly]@MOF-177 (Figure 1b) and 30-[Emim][Ala]@MOF-177 (Figure 1d). This progressive breakdown could be attributed to the surface association that took place between MOF-177 and the incorporated AAILs.

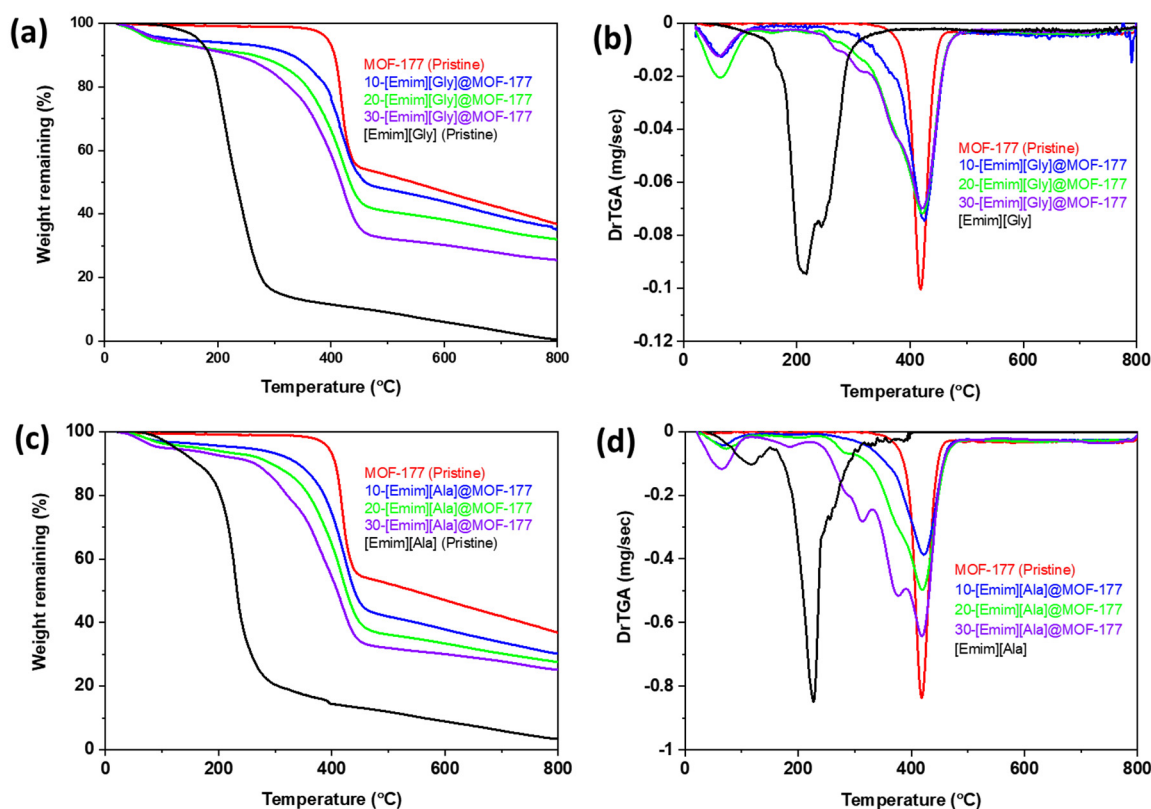


**Figure 1.** TGA thermograms and derivative of the TGA profiles of the compounds (a,b) [Emim][Gly]@MOF-177 and (c,d) [Emim][Ala]@MOF-177.

In an attempt to determine the effect that encapsulated AAILs had on the solid support of MOF-177, the crystal structure of the composites was investigated utilizing X-ray diffraction (XRD), and the results of this investigation are illustrated in Figure 2. In the diffractogram of pristine MOF-177, the main characteristic peaks were observed at  $5.5^\circ$ ,  $6.2^\circ$ ,  $9.6^\circ$ ,  $10.4^\circ$ , and  $11.3^\circ$ . A similar pattern was reported in the literature by Li and Yang [38], and major peaks were observed at  $5.2^\circ$ ,  $4.7^\circ$ , and  $6.2^\circ$  by Saha and Deng [37] and at  $5.5^\circ$  and  $6.2^\circ$  by Santos et al. [39]. As displayed in Figure 2a,b, the XRD of the composites revealed that the impregnation of AAILs into the MOF-177 support had a significant impact on peak intensity and position. For a low loading of 10 wt.% for both [Emim][Gly] and [Emim][Ala], the prominent characteristic peaks at  $5.5^\circ$ ,  $6.2^\circ$ , and  $9.6^\circ$  for pristine MOF-177 showed a significant decline, but the peaks at  $11.1^\circ$  and  $11.7^\circ$  retained their intensity, with a minor shift from the original positions. It was evident that the intensity of the major peaks diminished with the increment in AAILs' loading and eventually almost disappeared at a loading of 30 wt.%, as displayed for both 30-[Emim][Gly]@MOF-177 and 30-[Emim][Ala]@MOF-177. This diminishment and disappearance of these peaks can be attributed to the interaction between amine groups and MOF-177-Zn. Another factor that cannot be entirely disregarded is the potential degradation of the MOF framework's structure to some extent due to the exposure to the amine solution [40]. A similar phenomenon of a decrease in the intensity of the characteristic peaks of MOF-177 due to impregnation with polyethyleneimine (PEI) was reported by Gaikwad and co-workers [41]. Their XRD data also revealed a further decline in peak intensity with the increase in the loading of PEI and eventually almost the disappearance of the peaks at 30 wt.% PEI loading. This pattern was also observed for PEI@Cu-BTC (HKUST) composites [42], polyamine@MIL-101(Cr) [43], and PEI@MCM-41 [44]. The TGA thermograms discussed in the preceding section confirmed that there was a significant interaction between AAILs and the MOF-177 support. It is important to acknowledge that additional investigation would be beneficial to examine the structural integrity of MOF-177,

utilizing single-crystal XRD and scanning electron microscopy (SEM) subsequent to the exposure to a solvent under different conditions.

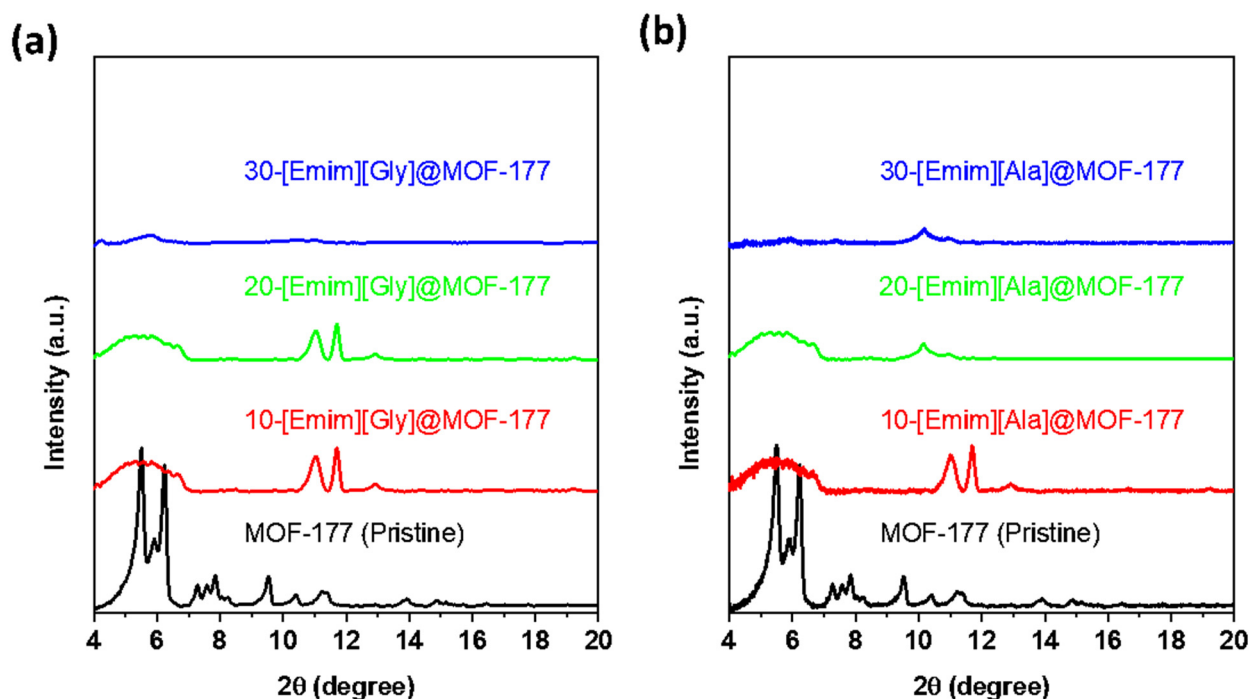


**Figure 2.** XRD profiles of pristine MOF-177 and the composites (a) Emim][Gly]@MOF-177 and (b) [Emim][Ala]@MOF-177.

To further assess the impact of the incorporation of AAILs on the textural properties of the MOF-177 support,  $N_2$  adsorption–desorption isotherms were obtained in a liquid nitrogen environment (77 K) using the ASAP 2460 analyzer (Micromeritics) for the unmodified MOF-177 and AAILs@MOF-177 composites, and the isotherms are presented in Figure 3. The samples' specific surface areas were determined at relative pressures ( $P/P_0$ ) between 0.04 and 0.1 bar using the Brunauer–Emmett–Teller (BET) model. In addition, the Langmuir surface area was calculated, and the results are presented in Table 1. The Hovath–Kawazoe (HK) model was used to calculate the pore size distribution for all the composites, and the results are displayed in Figure 4. The pristine MOF-177 showed a significantly higher  $N_2$  uptake, and the isotherm profile corresponded to a reversible type I isotherm (IUPAC classification), which was indicative of a microporous material lacking hysteresis during desorption. The BET and Langmuir surface areas of pristine MOF-177 were  $4172 \text{ m}^2 \cdot \text{g}^{-1}$  and  $4962 \text{ m}^2 \cdot \text{g}^{-1}$ , respectively, close to the reported values by Yaghi's group [35]. Both BET and Langmuir surface areas of MOF-177 reported in the literature varied significantly from  $3100$  to  $4962 \text{ m}^2 \cdot \text{g}^{-1}$  and from  $4300$  to  $5994 \text{ m}^2 \cdot \text{g}^{-1}$ , respectively [35,37,38,45]. It is shown in Figure 3 that  $N_2$  adsorption in all composites was significantly lower than in pristine MOF-177, which is evidence of a substantial drop in surface area as well as in pore volume (Table 1). For instance, upon impregnation with 10 wt.% [Emim][Gly] and [Emim][Ala], the BET surface areas were reduced to only  $187 \text{ m}^2 \cdot \text{g}^{-1}$  and  $152 \text{ m}^2 \cdot \text{g}^{-1}$ , respectively. The surface area and pore volume of the composites were further reduced with the addition of AAILs. The BET surface areas and pore volumes obtained for a 30 wt.% loading of [Emim][Gly] were estimated to be  $27 \text{ m}^2 \cdot \text{g}^{-1}$  and  $0.02 \text{ cm}^3 \cdot \text{g}^{-1}$ , respectively. These results indicated that the pores were almost filled. It should be acknowledged that the [Emim][Gly]@MOF-177 composites exhibited somewhat higher surface area and pore volume compared to the [Emim][Ala]@MOF-177 composites. The reduction in surface area and pore volume confirmed that the AAILs were encapsulated into the pores of MOF-177, which was also confirmed by XRD analysis in the previous section. As the loading of AAILs rose, there was a corresponding increase in the likelihood of pore blockage, as also evident

in the pore size distribution (Figure 4). Consequently, certain pores became inaccessible for  $N_2$  adsorption, which led to a reduction in pore volume. Similar observations were reported for PEI@UiO-66-NH<sub>2</sub> [40].

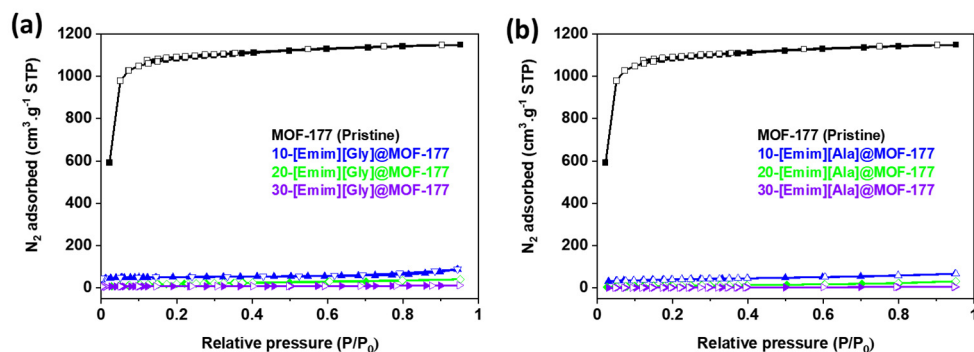


**Figure 3.**  $N_2$  adsorption–desorption isotherms at 77 K for unmodified MOF-177 and the composites (a) [Emim][Gly]@MOF-177 and (b) [Emim][Ala]@MOF-177. Filled and unfilled symbols represent adsorption and desorption isotherms, respectively.

**Table 1.** Textural properties of pristine MOF-177 and AAILs@MOF-177 composites computed from the  $N_2$  adsorption–desorption isotherms at 77 K.

Samples	$S_{BET}$ ( $m^2 \cdot g^{-1}$ )	$S_{Langmuir}$ ( $m^2 \cdot g^{-1}$ )	Pore Volume ( $cm^3 \cdot g^{-1}$ )
MOF-177	4172	4962	1.78
10-[Emim][Gly]@MOF-177	187	250	0.13
20-[Emim][Gly]@MOF-177	74	147	0.06
30-[Emim][Gly]@MOF-177	27	41	0.02
10-[Emim][Ala]@MOF-177	152	226	0.10
20-[Emim][Ala]@MOF-177	39	89	0.05
30-[Emim][Ala]@MOF-177	9.3	29	0.01

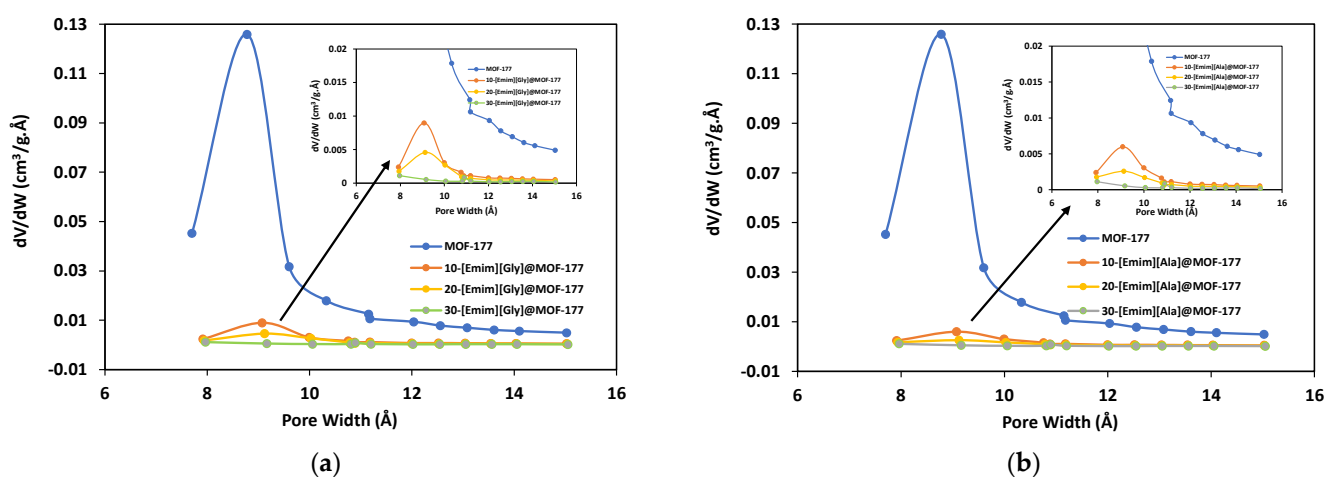


**Figure 4.** Pore size distribution for pristine MOF-177 and the composites (a) [Emim][Gly]@MOF-177 and (b) [Emim][Ala]@MOF-177.

## 2.2. CO<sub>2</sub> Adsorption Isotherms

MOF-177 is one of the most highly porous MOFs reported to date in the open literature and, as a result, it has higher adsorption capacity at high pressure. However, its adsorption capacity in post-combustion conditions (up to 0.15 bar) is very low [13]. The current investigation involved the synthesis of composites including [Emim][Gly]@MOF-177 and [Emim][Ala]@MOF-177. These composites were prepared by introducing two amino acid



anion-functionalized ionic liquids (AAILs), commonly referred to as task-specific ionic liquids (TSILs), into MOF-177 using the wet impregnation method. These composites' equilibrium CO<sub>2</sub> uptakes were determined at 30, 40, and 50 °C. The isotherms were obtained at pressures between 0.1 and 10 bar. Figure 5 shows the equilibrium CO<sub>2</sub> uptake in pure MOF-177 and [Emim][Gly]@MOF-177 for pressures spanning from 0.1 to 10.0 bar (Figure 5a,c,e) and a narrower pressure range (Figure 5b,d,f) from 0.1 to 1.0 bar. The addition of [Emim][Gly] to MOF-177 increased its ability to adsorb CO<sub>2</sub> at low pressures between 0.1 and 1.0 bar. When compared to those of pristine MOF-177 and all other [Emim][Gly]@MOF-177 composites at all temperatures, the CO<sub>2</sub> adsorption capacity increased dramatically with the incremental addition of AAIL loading and peaked at a loading of 20 wt%. At 0.2 bar and 303 K, the CO<sub>2</sub> adsorption for 20-[Emim][Gly]@MOF-177 was 0.45 mmol·g<sup>-1</sup> of solid, which was three times that of pristine MOF-177 under the same circumstances. However, increasing the TSIL amount to 30 wt.% failed to result in a noticeable rise in CO<sub>2</sub> uptake; rather, a decrease in CO<sub>2</sub> uptake to 0.26 mmol·g<sup>-1</sup> of solid was observed when compared to that observed with the 20 wt.% loading, even though it was a bit higher when compared to that of pure MOF-177 in the same conditions. It is noteworthy that the carbon dioxide absorption capacity of all [Emim][Gly]@MOF-177 composites exhibited a decrease in performance at the given temperature in comparison to pure MOF-177 when the pressure exceeded 2 bar. The CO<sub>2</sub> uptake by all composites decreased when the temperature was elevated from 30 °C to 40 °C and 50 °C while maintaining the same pressure.

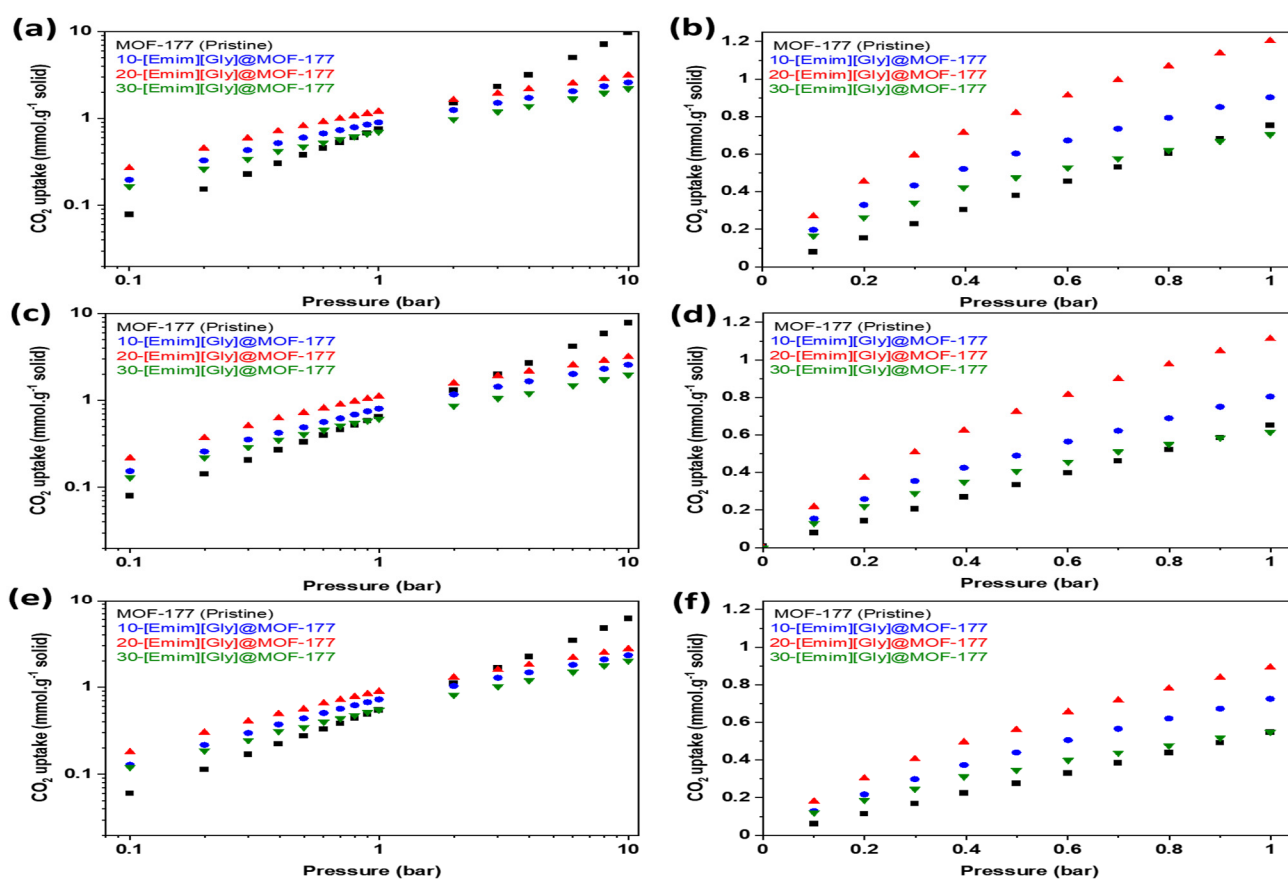


**Figure 5.** CO<sub>2</sub> equilibrium adsorption capacity of [Emim][Gly]@MOF-177 composites at two pressure ranges (0–10 bar and 0–1 bar) and three temperatures, i.e., (a,b) 303 K, (c,d) 313 K, and (e,f) 323 K.

Figure 6 shows the equilibrium CO<sub>2</sub> uptake in pure MOF-177 and [Emim][Ala]@MOF-177 for pressures spanning from 0.1 to 10.0 bar (Figure 6a,c,e) and a narrower pressure range (Figure 6b,d,f) from 0.1 to 1.0 bar. It demonstrates that the incorporation of [Emim][Ala] led to a favorable CO<sub>2</sub> adsorption capability at pressures below 2 bar, similar to what was observed for the [Emim][Gly]@MOF-177 composites. The composite 20-[Emim][Ala]@MOF-

177 outperformed all other [Emim][Ala]@MOF-177 composites and pure MOF-177 in CO<sub>2</sub> capture capacity. This composite reached an absorption capacity of 0.42 mmol·g<sup>-1</sup> of solid at 0.2 bar and 303 K, which was nearly three times higher than that of pristine MOF-177 under the same conditions. When the loading of [Emim][Ala] was raised to 30 wt.%, the CO<sub>2</sub> capture capacity decreased, and the resulting values were in the middle of the capture capacity range determined for the 10 and 20 wt.% loadings. It is worth noting that under identical temperatures and pressures, the CO<sub>2</sub> adsorption capacity of the [Emim][Ala]@MOF-177 composites was slightly lower than that of the [Emim][Gly]@MOF-177 composites for similar AAIL loadings.

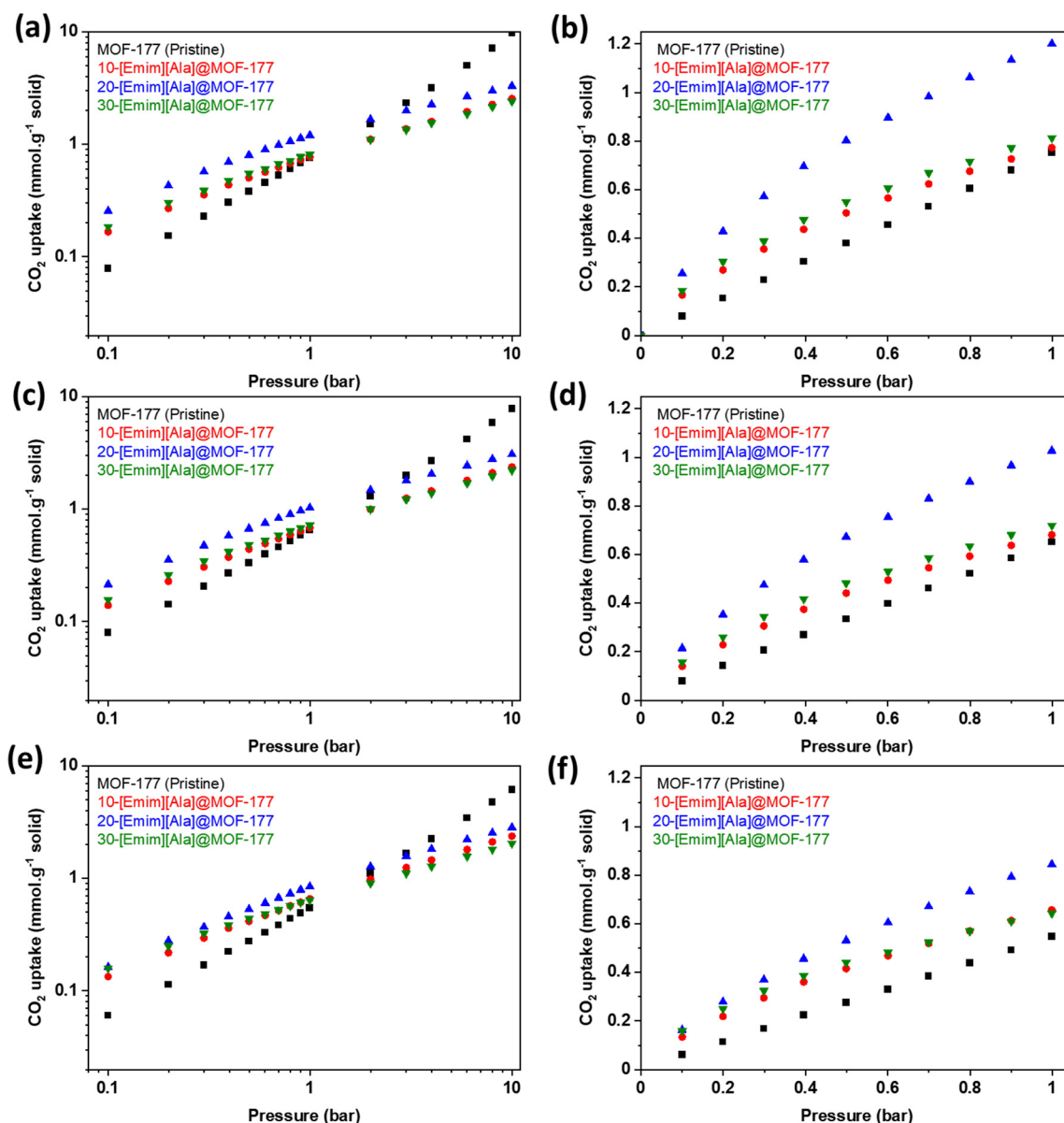
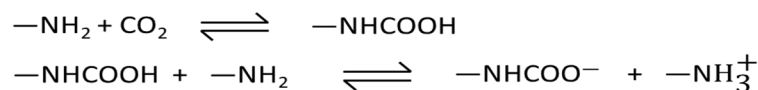


**Figure 6.** CO<sub>2</sub> equilibrium adsorption capacity of [Emim][Ala]@MOF-177 in two pressure ranges (0–10 bar and 0–1 bar) and three temperatures, i.e., (a,b) 303 K, (c,d) 313 K, and (e,f) 323 K.

The introduction of [Emim][Gly] and [Emim][Ala] AAILs to the MOF-177 sorbent led to a notable enhancement in CO<sub>2</sub> adsorption under post-combustion circumstances ( $P_{\text{CO}_2} \approx 0.15$  bar) due to the strong attraction between CO<sub>2</sub> and the amino group present in AAILs. Previous research indicated that the amino group of AAILs reacted with CO<sub>2</sub> via a process analogous to that of amines dissolving in water [26,46,47]. Wang et al. [48] suggested that as the cation and anion of [Emim][Gly] are small in size, they could come

nearby an amino group and react with it to form a carbamate with a stoichiometry of 1:2 (Scheme 1). Hence, it is reasonable to assume that the amino group present in these composites reacted with CO<sub>2</sub> to form a carbamate, resulting in a higher CO<sub>2</sub> capture capacity compared to pure MOF-177 below 1 bar.



**Scheme 1.** Schematics of the reaction of CO<sub>2</sub> with an amino-containing ionic liquid (AAIL) impregnated in a solid support [46].

It is noteworthy to mention that, when the pressure was below 1 bar, chemical absorption prevailed. This was attributed to the strong affinity between CO<sub>2</sub> and AAILs, consequently resulting in CO<sub>2</sub> absorption capacity enhancement. However, it is important to note that the occupation of the MOF-177 pores by AAILs molecules led to a significant reduction in the available surface area of the composites. Nevertheless, as the pressure increased, the composites' advantages were lost, resulting in a CO<sub>2</sub> uptake that was lower than that of pristine MOF-177 at pressures exceeding 2 bar. This decline could be due to the significant reduction in pore volume as well as the surface area of the composites. At moderate to high pressure, the absorption capacity of a sorbent is primarily influenced by physical parameters, in addition to the active chemical adsorption sites [49].

Our experimental results revealed that there was an upper limit to the loading of AAILs in relation to the enhancement of CO<sub>2</sub> absorption, which was found to be 20 wt.%; beyond that limit, the CO<sub>2</sub> uptake decreased. This reduction in CO<sub>2</sub> capacity was ascribed to the reduction in accessible active sites in the sorbent due to the blockage created by the high AAIL concentrations, which was also evidenced by the BET surface area and pore volume results obtained for 30 wt.% AAILs@MOF-177, as discussed earlier. An analogous finding was reported by Wang et al. [48] for the impregnation of [Emim][Gly] into the nanoporous structure of polymethylmethacrylate (PMMA) by varying the loading from 0 to 100 wt.%; the optimum loading was found to be 50 wt.%. In another study, Uehara et al. [32] reported that the optimum loading of [Emim][Lys] was 60 wt.% for the mesoporous silica support SBA-15.

The stability of the composites in the CO<sub>2</sub> capture operation was investigated by performing multiple cycles of adsorption at 313 K and desorption at 373 K at the atmospheric pressure in the presence of N<sub>2</sub> for 20 wt.%-[Emim][Gly]@MOF-177, using an IGA microbalance. The obtained results are displayed in Figure 7. They showed that the composite sorbent could almost maintain its original adsorption capacity during multicycle operations. In addition, the CO<sub>2</sub> uptake process for AAILs@MOF-177 was completely reversible, suggesting that the composites could be readily regenerated in the presence of flowing N<sub>2</sub> at 100 °C.

### 2.3. Selectivity for CO<sub>2</sub>/N<sub>2</sub>

To be deemed effective in the post-combustion capture of carbon dioxide (CO<sub>2</sub>), a solid sorbent must have a notable level of selectivity towards CO<sub>2</sub> compared to nitrogen (N<sub>2</sub>). Consequently, the determination of N<sub>2</sub> adsorption isotherms at 40 °C was undertaken to quantify the CO<sub>2</sub>/N<sub>2</sub> selectivity. Each isotherm encompassed a range of pressures ranging from 0.1 to 10 bar. In our current study, we employed a particular methodology to determine the optimal selectivity. Our strategy entailed calculating the selectivity by comparing the molar uptakes of individual components at a given pressure, according to Equation (1) [2]:

$$S = \frac{q_{\text{CO}_2}}{q_{\text{N}_2}} \quad (1)$$

where S denotes the selectivity, and q<sub>CO<sub>2</sub></sub> and q<sub>N<sub>2</sub></sub> represent the molar uptakes of CO<sub>2</sub> and N<sub>2</sub>, respectively. Figure 8 presents the results of the calculations of CO<sub>2</sub>/N<sub>2</sub> selectivity for both [Emim][Gly]@MOF-177 and [Emim][Ala]@MOF-177 composites. Throughout the



whole pressure spectrum, the  $\text{CO}_2/\text{N}_2$  selectivity of pure MOF-177 fluctuated between the values of 3 and 5. It was discovered that the impregnation of [Emim][Gly] and [Emim][Ala] into MOF-177 boosted the selectivity for all loadings compared to that of the virgin MOF-177 up to a pressure of 2 bar. As for [Emim][Gly]@MOF-177, it was observed that the compound 20-[Emim][Gly]@MOF-177 demonstrated the highest selectivity, reaching a value of about 13 at a pressure of 0.2 bar and a temperature of 313 K. Nevertheless, the observed value exhibited a gradual decline as the pressure was raised, as depicted in Figure 8a. It is important to note that the increase in AAIL loading to 30-[Emim][Gly] did not increase the selectivity; rather, it resulted in a selectivity that was worse than that observed for the 10 wt.% loading, except at 0.1 bar. A similar behavior was seen for the [Emim][Ala]@MOF-177 composites, with maximum selectivity of around 15 (0.1 bar) and 11 (0.2 bar) displayed by 20-[Emim][Ala]@MOF-177. It was discovered, however, that the selectivity of the 30-[Emim][Ala]@MOF-177 composite was nearly identical to that of the 20-[Emim][Ala]@MOF-177 composite.

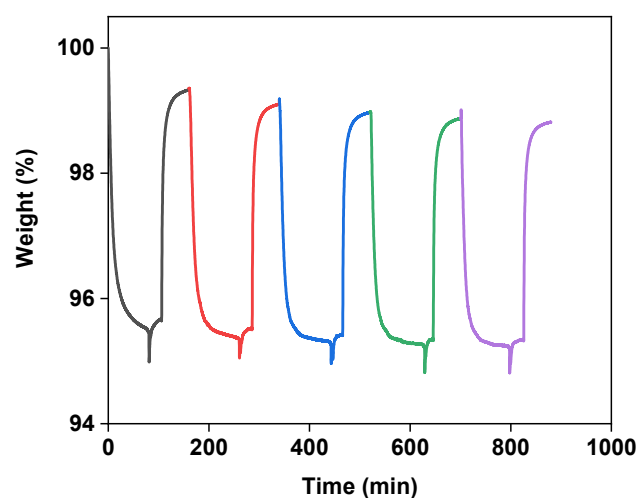


**Figure 7.** Adsorption and desorption performance during multiple cycles of the 20 wt.% [Emim][Gly]@MOF-177 composite. The adsorption was conducted at 313 K, and the desorption at 373 K in the presence of a flow of  $\text{N}_2$ .

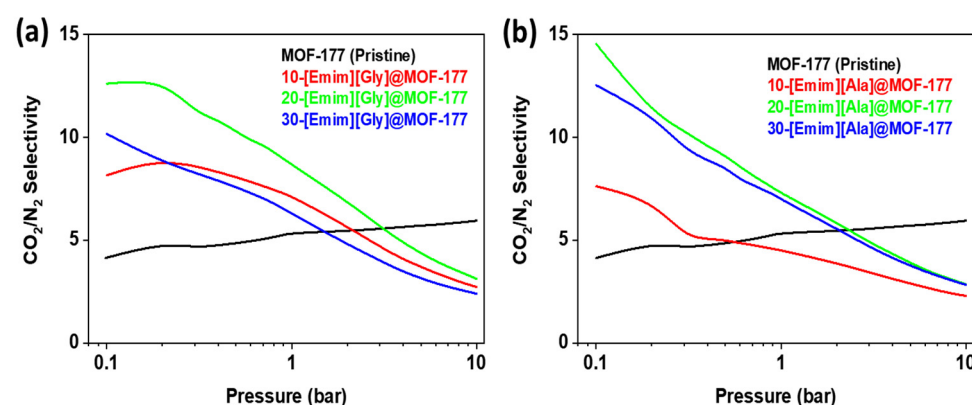


**Figure 8.**  $\text{CO}_2/\text{N}_2$  selectivity of the (a) [Emim][Gly]@MOF-177 and (b) [Emim][Ala]@MOF-177 composites at 313 K.

The encapsulated amino acid-base ionic liquids contributed to the enhancement of  $\text{CO}_2/\text{N}_2$  selectivity. This improvement was observed at pressures below 2 bar. As previously discussed, it was proposed that the presence of amino acids leads to the formation of active chemical sorption sites for  $\text{CO}_2$ , facilitating the creation of an N-C bond. This interaction is similar to that observed when  $\text{CO}_2$  interacts with an aqueous amine solution [46,48]. In our work, it resulted in additional  $\text{CO}_2$  capture, although the surface areas and pore

volumes were reduced due to the addition of the ionic liquid. On the other hand, N<sub>2</sub> did not have an affinity for the amino group as the adsorption was physical and depended on the available surface area. Hence, CO<sub>2</sub> uptake was dominant at low pressure compared to N<sub>2</sub> uptake, resulting in higher CO<sub>2</sub>/N<sub>2</sub> selectivity. However, as the pressure increased, the physical adsorption sites also became determining factors of the adsorption capacity besides the active chemical adsorption sites in the sorbent. Consequently, the CO<sub>2</sub>/N<sub>2</sub> selectivity of the composites decreased as the pressure increased and became lower than that of pristine MOF-177 at pressures above 2 bar.

The CO<sub>2</sub>/N<sub>2</sub> selectivity and CO<sub>2</sub> uptake of the examined composites, along with those reported in our previous studies and for other composites in the literature, are presented in Table 2. It is evident that the CO<sub>2</sub> uptake and CO<sub>2</sub>/N<sub>2</sub> selectivity of the best-performing composite, AAILs@MOF-177 (20%), were lower than those of our previously reported best-performing AAIL composites containing a ZIF-8 support (30%). These composites also performed better than some of the reported composites in the literature. An even better performance was expected for AAILs@MOF-177, given the porosity of pristine MOF-177; however, the host–guest interactions in a composite, the guest molecules' loading, the support's stability, the composite's porosity significantly influence the CO<sub>2</sub> adsorption capacity.

**Table 2.** CO<sub>2</sub> uptake and selectivity of various composites reported in the literature.

Composites	CO <sub>2</sub> Uptake (mmol g <sup>-1</sup> )	CO <sub>2</sub> /N <sub>2</sub> Selectivity <sup>a</sup>	Experimental Conditions	Ref.
20-[Emim][Gly]@MOF-177	0.45	13	0.2 bar/303 K	This work
20-[Emim][Ala]@MOF-177	0.42	11	0.2 bar/303 K	This work
10-[Emim][Ac]@MOF-1777	0.38	-	0.2 bar/303 K	[36]
30-[Bmim][Ac]@ZIF-8	0.8 <sup>b</sup>	12	0.2 bar/303 K	[50]
30-[Emim][Ac]@ZIF-8	0.7 <sup>b</sup>	4	0.2 bar/303 K	[50]
30-[Emim][Gly]@ZIF-8	0.89	19 <sup>c</sup>	0.2 bar/303 K	[34]
30-[Emim][Ala]@ZIF-8	0.91	8 <sup>c</sup>	0.2 bar/303 K	[34]
2.5-PEI-CuBTC (HKUST)	0.45		0.15 bar/313 K	[42]
30-[Bmim][PF6]@ZIF-8	0.18 <sup>b</sup>	17	0.2 bar/298 K	[24]
25-[Bmim][BF4]@ZIF-8	0.09 <sup>b</sup>	13	0.2 bar/298 K	[25]

<sup>a</sup> Ideal selectivity unless stated otherwise; <sup>b</sup> values were retrieved from the graph and calculated as mmol g<sup>-1</sup> from cm<sup>3</sup> g<sup>-1</sup> (STP); <sup>c</sup> selectivity at 313 K.

#### 2.4. Equilibrium Isotherm Modeling

To accurately represent the outcomes of the experimental investigations pertaining to the design of adsorption and desorption processes, it was imperative to construct a model of the equilibrium isotherm. The presence of encapsulated AAILs within the pore structure of MOF-177 resulted in the composite material under investigation exhibiting binding sites of varying strengths. After conducting a comparative analysis with various existing models, it was determined that the dual-site Langmuir (DSL) model [24,50] had a high level of suitability. The model incorporates the Langmuir adsorption mechanism, which involves two distinct adsorption sites. The overall adsorption is determined by the cumulative adsorption, involving the absorption occurring at each individual site, as represented by Equation (2) [1]:

$$N_e = \frac{N_A b_A P}{1 + b_A P} + \frac{N_B b_B P}{1 + b_B P} \quad (2)$$

In the DSL model, the equilibrium intake of CO<sub>2</sub> ( $N_e$ ) is denoted in millimoles per gram of solid, while the equilibrium pressure ( $P$ ) is given in bar. The parameters  $N_A$ ,  $N_B$ ,  $b_A$ , and  $b_B$  were regressed using the model. Their values are presented in Tables 3 and 4. These tables include the parameters obtained from the regression analysis for different loadings of ionic liquids (ILs) at various temperatures. Figures 9 and 10 provide visual

representations of the fitting curves generated by the DSL model. Due to the  $R^2$  values exhibiting a high degree of proximity to unity, the model effectively achieved a remarkable level of conformity with the experimental data. Consequently, the data obtained from the model were utilized to compute the heat of adsorption in the subsequent section.

**Table 3.** Computed parameters of the DSL model for the [Emim][Gly]@MOF-177 composites with different loadings of AAILs for pressures spanning from 0.1 to 2.0 bar.

Model Parameters	10-[Emim][Gly]@ MOF-177			20-[Emim][Gly]@MOF-177			30-[Emim][Gly]@MOF-177		
	30 °C	40 °C	50 °C	30 °C	40 °C	50 °C	30 °C	40 °C	50 °C
$N_A$	2.019	2.350	1.921	0.436	0.292	0.165	1.590	0.097	0.087
$b_A$	0.514	0.426	0.562	5.117	4.698	9.030	0.508	10.678	18.396
$N_B$	0.247	0.098	0.024	2.371	2.694	2.444	0.190	1.405	1.628
$b_B$	6.692	15.04	10,000	0.545	0.479	0.439	8.468	0.609	0.404
$R^2$	1.000	1.000	1.000	1.000	1.000	1.000	1.000	1.000	1.000

**Table 4.** Computed parameters of the DSL model for the [Emim][Ala]@MOF-177 composites with different loadings of AAILs for pressures spanning from 0.1 to 2.0 bar.

Model Parameters	10-[Emim][Ala]@ MOF-177			20-[Emim][Ala]@MOF-177			30-[Emim][Ala]@MOF-177		
	30 °C	40 °C	50 °C	30 °C	40 °C	50 °C	30 °C	40 °C	50 °C
$N_A$	1.960	0.000	0.151	0.306	0.230	2.791	1.698	1.602	0.246
$b_A$	0.501	0.000	7.765	6.003	7.147	0.326	0.697	0.539	7.046
$N_B$	0.129	1.600	2.182	2.607	2.618	0.185	0.122	0.180	1.599
$b_B$	12.735	0.763	0.315	0.564	0.462	6.700	15.549	6.987	0.365
$R^2$	1.000	0.999	1.000	1.000	1.000	1.000	1.000	1.000	1.000

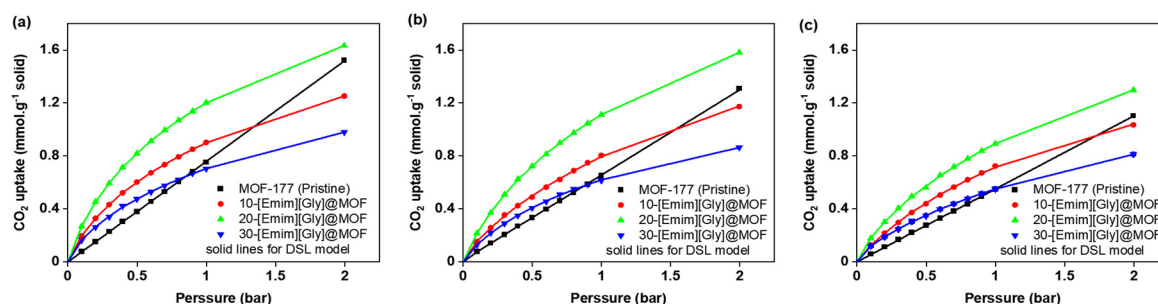


**Figure 9.** Fitting of the DSL model for MOF-177 and the [Emim][Gly]@ MOF-177 composites with different loadings of AAILs at (a) 30 °C, (b) 40 °C, and (c) 50 °C for pressures spanning from 0.1 to 2.0 bar.

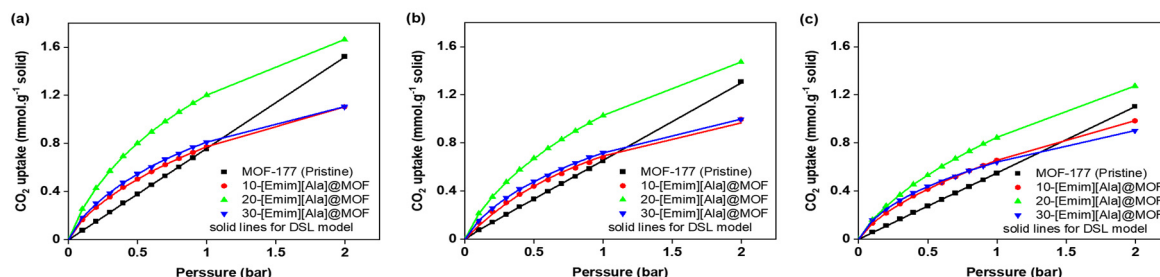


**Figure 10.** Fitting of the DSL model for MOF-177 and the [Emim][Ala]@ MOF-177 composites with different loadings of AAILs at (a) 30 °C, (b) 40 °C, and (c) 30 °C for pressures spanning from 0.1 to 2.0 bar.

### 2.5. Isostatic Heat of Adsorption ( $Q_{st}$ )

The determination of the adsorption enthalpy of carbon dioxide ( $Q_{st}$ ), referred to as the isosteric heat of adsorption, plays a pivotal role in the adsorption process. It displays

the gas molecules' affinity for the adsorbents and the degree of their interaction. The energy requirements for the adsorption–desorption process were therefore quantified. The CO<sub>2</sub> isotherms at (303, 313, and 323) K were used to calculate the adsorption enthalpy ( $Q_{st}$ ). At first, the DSL model was employed to establish a suitable match for the isotherms, as discussed in the preceding section. Subsequently, the Clausius–Clapeyron Equation (3) was utilized [1]

$$(\ln P)_N = -\left(\frac{Q_{st}}{R}\right)\left(\frac{1}{T}\right) + C \quad (3)$$

In the given context, the symbol  $P$  denotes the pressure in bar,  $N$  represents the extent of CO<sub>2</sub> adsorption,  $T$  signifies the temperature measured in Kelvin (K), and  $R$  denotes the universal gas constant. The equation was utilized to produce graphs depicting the natural logarithm of the partial pressure ( $\ln P$ ) as a function of the reciprocal of temperature ( $1/T$ ) while maintaining a constant rate of carbon dioxide consumption. The value of  $Q_{st}$  was then determined by calculating the slope of these plots. The findings are depicted in Figure 11, illustrating the outcomes for both pure MOF-177 and AAILs@MOF-177.

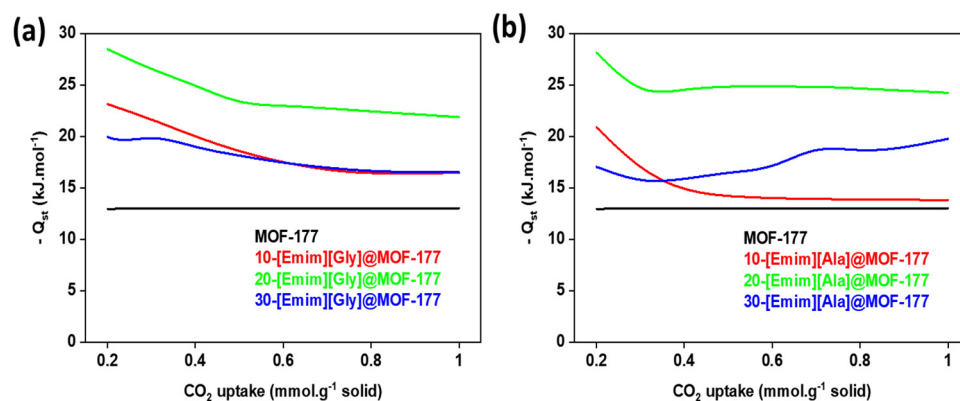


**Figure 11.** The enthalpy of CO<sub>2</sub> adsorption ( $Q_{st}$ ) of the composites (a) [Emim][Gly]@MOF-177 and (b) [Emim][Ala]@MOF-177.

The  $Q_{st}$  values for the pure MOF-177 remained relatively stable at 13 kJ·mol<sup>−1</sup>. In contrast, a significant rise in  $Q_{st}$  was observed for the composites, particularly at low levels of CO<sub>2</sub> uptake. When compared to other [Emim][Gly] composites, 20-[Emim][Gly]@MOF-177 showed the highest values for  $Q_{st}$ , reaching a maximum of −28 kJ·mol<sup>−1</sup> at 0.2 mmol·g<sup>−1</sup> CO<sub>2</sub> uptake. This value was double that of pure MOF-177 under identical conditions (Figure 11a). Similarly, it was observed that the composite material 20-[Emim][Ala]@MOF-177 displayed the highest  $Q_{st}$  values compared to the other [Emim][Ala]@MOF-177 composites (Figure 11b). The significant increase in  $Q_{st}$  can be ascribed to the strong intermolecular forces between carbon dioxide (CO<sub>2</sub>) and the ionic liquids that had been incorporated within the pores of MOF-177. There exists a hypothesis suggesting that the anions of AAILs, containing the -NH<sub>2</sub> group, undergo a reaction to form an N-C bond. This reaction is believed to contribute to the higher heat release observed after the adsorption of CO<sub>2</sub> [48]. The decrease in the quantity of available adsorption sites can be attributed to the observed decline in the  $Q_{st}$  value across all composites, which coincided with an increase in CO<sub>2</sub> uptake. A similar observation was reported for a composite of MIL-100 (Fe) modified with DETA [18]. As expected, the  $Q_{st}$  values for both 30%-[Emim][Gly]@MOF-177 and 30%-[Emim][Ala]@MOF-177 were between those for the 10 and 20 wt.% loadings, which confirmed the CO<sub>2</sub> adsorption isotherm and selectivity pattern observed and discussed in the previous section.

### 3. Materials and Methods

#### 3.1. Materials

Sigma Aldrich supplied methanol (CAS 67-56-1), [Emim][Gly] (CAS 766537-74-0), [Emim][Ala] (CAS 766537-81-9), and MOF-177 (basolite Z377, CAS: 676593-65-0). Before

beginning the sample preparation, MOF-177 was allowed to dry overnight at 110 °C. All other compounds were used as supplied. To reduce the amount of time that the samples were exposed to moisture, the ionic liquid, MOF-177, and the produced composites were stored in a glovebox (Clean Tech LLC, Minot, ND, USA) filled with argon gas. Praxair Inc. Canada (Mississauga, ON, Canada) was the supplier of CO<sub>2</sub> and N<sub>2</sub>, which had a high purity level (99.99 vol.%).

### 3.2. Preparation of the AAIL@MOF-177 Composites

Using the wet impregnation approach and methanol as a solvent, amino acid ionic liquids [Emim][Gly] and [Emim][Ala] were effectively embedded within the porous MOF-177 support. In summary, the desired amount of AAILs was added to 4 mL of methanol in a small glass vial, and the mixture was homogenized by shaking it for 30 min. The AAIL–methanol solution was carefully added in a dropwise manner to the pre-weighed dehydrated MOF-177, which was contained in a separate glass vial. The resulting combination was then agitated for 1 h. Following 24 h of solvent evaporation under ambient conditions, any residual solvent was removed by subjecting the composite to a drying process at a temperature of 80 °C, well above the boiling point of methanol (65 °C), for 2 h. The created composite samples were stored in an argon-filled glovebox to prevent exposure to moisture and were labelled as X-AAILs@MOF-177, in which X represents the weight % of AAILs used; for instance, 10 wt.% [Emim][Gly] is here referred to as 10-[Emim][Gly]@MOF-177.

### 3.3. Characterization

The thermogravimetric analysis (TGA) of [Emim][Gly], [Emim][Ala], pristine MOF-177, and all synthesized AAILs@MOF-177 composites was conducted with a Shimadzu Thermal Gravimetric Analysis device (TGA-50). The analysis was performed using a nitrogen flow rate of 50 mL/min with the temperature gradually increasing to 800 °C at a rate of 10 °C/min. In each of the analyses, a sample amount of roughly 10 to 12 mg was utilized. To analyze the crystal structure of the pure MOF-177 support as well as of the AAILs@MOF-177 composites, a tabletop X-ray diffraction (XRD) device (Rigaku Miniflex-II) was employed. The Cu K $\alpha$  radiation used in this experiment had a wavelength of 1.5418 Å. The examination was carried out at a scanning step of 1.2 °C/min between 2 $\theta$  values of 2 and 20 degrees, a temperature of 77 K, and using an instrument manufactured by Micromeritics ASAP. The N<sub>2</sub> adsorption and desorption isotherms of MOF-177 and the as-synthesized composites were determined. Based on the data from the N<sub>2</sub> isotherm, the textural features of each sample, such as the surface area (BET and Langmuir) as well as the pore volume, were computed.

### 3.4. Adsorption Isotherms

An intelligent gravimetric analyzer (IGA-003), manufactured by Hidden Isochema Ltd. (Warrington, UK), was utilized to acquire CO<sub>2</sub> adsorption data at 303, 313, and 323 K, as well as N<sub>2</sub> adsorption data at 313 K, throughout a wide span of pressures ranging from 0.1 bar to 10 bar. The IGA consisted of a computer-controlled microbalance that measured the weight in real time with a precision of 1 µg. Between 50 and 70 mg of material were deposited into a sample bucket for each isotherm. After heating the sample chamber to 80 °C using a water bath and vacuuming to 10 mbar with a diaphragm and turbo-pump (Pfeiffer, Asslar, Germany), the sample weight stayed constant for 1 h, indicating that all the solvent, moisture, and contaminants were removed. Following the completion of the outgassing process, the temperature of the water bath was adjusted to the predetermined isotherm temperature, and subsequently, the sample was permitted to attain the designated temperature. Once the sample was ready, the pressure level was pre-set to a value ranging from 0.1 to 10 bar in the IGASwin software (v.1.03.143), and the isotherm measurements were initiated. A mass flow controller (MFC) was used to regulate the quantity of CO<sub>2</sub> or N<sub>2</sub> injected into the chamber to maintain the desired pressure. The IGASwin program kept track of the real-time measurements of mass, temperature, and pressure. After allowing



each pressure level to establish equilibrium for at least two hours and recording the results, more CO<sub>2</sub> or N<sub>2</sub> was injected via the MFC at the following pressure level. At a given temperature, this procedure was repeated for each of the predetermined pressures. After the experiment was completed, the buoyancy effect was accounted for in the real-time adsorption data.

### 3.5. Cyclic Adsorption–Desorption Test

At 40 °C and 1 bar, the IGA was used to perform cyclic CO<sub>2</sub> adsorption and desorption studies. As explained earlier, first, the adsorption sample was degassed, and the temperature was adjusted to 40 °C. After 30 min to achieve temperature stabilization, the injection of carbon dioxide (100 mL/min) was carried out to commence the process of adsorption, maintained for 60 min. To facilitate the desorption, the sample was thereafter exposed to a thermal treatment at a temperature of 100 °C under a continuous flow of nitrogen gas (100 mL/min) for 150 min. This process aimed at eliminating the adsorbed carbon dioxide from the sample. These processes of adsorption and desorption were carried out for five cycles.

## 4. Conclusions

Enhanced CO<sub>2</sub> adsorption and selectivity were observed in composites made by encapsulating two amino acid-based ionic liquids (AAILs) within the highly porous metal-organic framework MOF-177. The composite material with a loading of 20 wt.% [Emim][Gly] demonstrated the highest recorded CO<sub>2</sub> uptake of 0.45 mmol·g<sup>-1</sup> of solid at a pressure of 0.2 bar and a temperature of 303 K. The composite material with 20 wt.% [Emim][Ala] exhibited a CO<sub>2</sub> uptake of 0.42 mmol·g<sup>-1</sup> of solid, three and 2.8 times higher than the CO<sub>2</sub> uptake of pure MOF-177. The introduction of AAILs resulted in an enhancement of the CO<sub>2</sub>/N<sub>2</sub> selectivity, with values increasing from 5 (for pure MOF-177) to 13 for [Emim][Gly] and 11 for [Emim][Ala] at a pressure of 0.2 bar and a temperature of 313 K. The interaction between carbon dioxide and the amino (-NH<sub>2</sub>) functional group, facilitated by the anion of the amino acid ionic liquids (AAILs), resulted in increased adsorption enthalpy ( $Q_{st}$ ) values. The  $Q_{st}$  values for pure MOF-177 remained relatively stable at 13 kJ·mol<sup>-1</sup>; in contrast, a significant rise in  $Q_{st}$  was observed for the composites, particularly at low levels of CO<sub>2</sub> uptake. When compared to other [Emim][Gly] composites, 20-[Emim][Gly]@MOF-177 showed the highest  $Q_{st}$  values, reaching a maximum of -28 kJ·mol<sup>-1</sup> at 0.2 mmol·g<sup>-1</sup> of CO<sub>2</sub> uptake. The present investigation also revealed that the ideal loading of AAIL was 20 wt.%, whereas any subsequent increase in loading to 30 wt.% was inadvisable. At a loading of 30 wt.%, the decline in CO<sub>2</sub> absorption could potentially be attributed to a reduction in the availability of active sites on the sorbent. This reduction could be caused by the blockage or a partial collapse of the MOF-177 structure, as evidenced by a decrease in both surface area and pore volume.

This study provides insights into the structural integrity of AAILs@MOF-177 composites, their performance in terms of CO<sub>2</sub> capture and CO<sub>2</sub>/N<sub>2</sub> selectivity, and their adsorption enthalpies in post-combustion CO<sub>2</sub> capture processes.

**Author Contributions:** F.A.P., conceptualization, methodology, material synthesis, characterization, experimental analysis, validation, data analysis, writing—original draft preparation; A.H., conceptualization, resources, funding acquisition, writing—review and editing—project administration, supervision. All authors have read and agreed to the published version of the manuscript.

**Funding:** This research was funded by a grant provided to the second author by the Natural Sciences and Engineering Research Council of Canada (NSERC)—Discovery Grant (RGPIN-2018-06805).

**Institutional Review Board Statement:** Not applicable.

**Informed Consent Statement:** Not applicable.

**Data Availability Statement:** The data presented in this study are available on request from the corresponding author.

**Acknowledgments:** The authors are grateful to Golam Kibria (University of Calgary) for providing support for some sample characterizations.

**Conflicts of Interest:** The authors declare no conflict of interest.

**Sample Availability:** Samples of the compounds are not available from the authors.

## References

1. Sumida, K.; Rogow, D.L.; Mason, J.A.; McDonald, T.M.; Bloch, E.D.; Herm, Z.R.; Bae, T.-H.; Long, J.R. Carbon Dioxide Capture in Metal–Organic Frameworks. *Chem. Rev.* **2012**, *112*, 724–781. [[CrossRef](#)]
2. Lin, Y.; Kong, C.; Zhang, Q.; Chen, L. Metal–Organic Frameworks for Carbon Dioxide Capture and Methane Storage. *Adv. Energy Mater.* **2017**, *7*, 1601296. [[CrossRef](#)]
3. Amaro-Gahete, J.; Klee, R.; Esquivel, D.; Ruiz, J.R.; Jiménez-Sanchidrián, C.; Romero-Salguero, F.J. Fast Ultrasound-Assisted Synthesis of Highly Crystalline MIL-88A Particles and Their Application as Ethylene Adsorbents. *Ultrason. Sonochem.* **2019**, *50*, 59–66. [[CrossRef](#)]
4. Li, H.; Wang, K.; Sun, Y.; Lollar, C.T.; Li, J.; Zhou, H.C. Recent Advances in Gas Storage and Separation Using Metal–Organic Frameworks. *Mater. Today* **2018**, *21*, 108–121. [[CrossRef](#)]
5. Rojas-Luna, R.; Amaro-Gahete, J.; Gil-Gavilán, D.G.; Castillo-Rodríguez, M.; Jiménez-Sanchidrián, C.; Ruiz, J.R.; Esquivel, D.; Romero-Salguero, F.J. Visible-Light-Harvesting Basolite-A520 Metal Organic Framework for Photocatalytic Hydrogen Evolution. *Microporous Mesoporous Mater.* **2023**, *355*, 112565. [[CrossRef](#)]
6. Zhao, Y.; Song, Z.; Li, X.; Sun, Q.; Cheng, N.; Lawes, S.; Sun, X. Metal Organic Frameworks for Energy Storage and Conversion. *Energy Storage Mater.* **2016**, *2*, 35–62. [[CrossRef](#)]
7. Zhu, L.; Liu, X.Q.; Jiang, H.L.; Sun, L.B. Metal–Organic Frameworks for Heterogeneous Basic Catalysis. *Chem. Rev.* **2017**, *117*, 8129–8176. [[CrossRef](#)]
8. Lawson, H.D.; Walton, S.P.; Chan, C. Metal–Organic Frameworks for Drug Delivery: A Design Perspective. *ACS Appl. Mater. Interfaces* **2021**, *13*, 7004–7020. [[CrossRef](#)]
9. Hu, Z.; Wang, Y.; Shah, B.B.; Zhao, D. CO<sub>2</sub> Capture in Metal–Organic Framework Adsorbents: An Engineering Perspective. *Adv. Sustain. Syst.* **2018**, *3*, 1800080. [[CrossRef](#)]
10. Aghaie, M.; Rezaei, N.; Zendejboudi, S. A Systematic Review on CO<sub>2</sub> Capture with Ionic Liquids: Current Status and Future Prospects. *Renew. Sustain. Energy Rev.* **2018**, *96*, 502–525. [[CrossRef](#)]
11. Yu, J.; Xie, L.H.; Li, J.R.; Ma, Y.; Seminario, J.M.; Balbuena, P.B. CO<sub>2</sub> Capture and Separations Using MOFs: Computational and Experimental Studies. *Chem. Rev.* **2017**, *117*, 9674–9754. [[CrossRef](#)] [[PubMed](#)]
12. Belmabkhout, Y.; Guillerm, V.; Eddaoudi, M. Low Concentration CO<sub>2</sub> Capture Using Physical Adsorbents: Are Metal–Organic Frameworks Becoming the New Benchmark Materials? *Chem. Eng. J.* **2016**, *296*, 386–397. [[CrossRef](#)]
13. Adil, K.; Bhatt, P.M.; Belmabkhout, Y.; Abtab, S.M.T.; Jiang, H.; Assen, A.H.; Mallick, A.; Cadiau, A.; Aqil, J.; Eddaoudi, M. Valuing Metal–Organic Frameworks for Postcombustion Carbon Capture: A Benchmark Study for Evaluating Physical Adsorbents. *Adv. Mater.* **2017**, *29*, 1702953. [[CrossRef](#)] [[PubMed](#)]
14. Yin, Z.; Wan, S.; Yang, J.; Kurmoo, M.; Zeng, M.H. Recent Advances in Post-Synthetic Modification of Metal–Organic Frameworks: New Types and Tandem Reactions. *Coord. Chem. Rev.* **2019**, *378*, 500–512. [[CrossRef](#)]
15. Jasuja, H.; Walton, K.S. Experimental Study of CO<sub>2</sub>, CH<sub>4</sub>, and Water Vapor Adsorption on a Dimethyl-Functionalized UiO-66 Framework. *J. Phys. Chem. C* **2013**, *117*, 7062–7068. [[CrossRef](#)]
16. Cmarik, G.E.; Kim, M.; Cohen, S.M.; Walton, K.S. Tuning the Adsorption Properties of UiO-66 via Ligand Functionalization. *Langmuir* **2012**, *28*, 15606–15613. [[CrossRef](#)]
17. Shearer, G.C.; Vitillo, J.G.; Bordiga, S.; Svelle, S.; Olsbye, U.; Lillerud, K.P. Functionalizing the Defects: Postsynthetic Ligand Exchange in the Metal Organic Framework UiO-66. *Chem. Mater.* **2016**, *28*, 7190–7193. [[CrossRef](#)]
18. Mutyala, S.; Yakout, S.M.; Ibrahim, S.S.; Jonnalagadda, M.; Mitta, H. Enhancement of CO<sub>2</sub> Capture and Separation of CO<sub>2</sub>/N<sub>2</sub> Using Post-Synthetic Modified MIL-100(Fe). *N. J. Chem.* **2019**, *43*, 9725–9731. [[CrossRef](#)]
19. Su, X.; Bromberg, L.; Martis, V.; Simeon, F.; Huq, A.; Hatton, T.A. Postsynthetic Functionalization of Mg-MOF-74 with Tetraethylenepentamine: Structural Characterization and Enhanced CO<sub>2</sub> Adsorption. *ACS Appl. Mater. Interfaces* **2017**, *9*, 11299–11306. [[CrossRef](#)]
20. Lin, Y.; Yan, Q.; Kong, C.; Chen, L. Polyethyleneimine Incorporated Metal–Organic Frameworks Adsorbent for Highly Selective CO<sub>2</sub> Capture. *Sci. Rep.* **2013**, *3*, 1859. [[CrossRef](#)]
21. Choi, S.; Watanabe, T.; Bae, T.H.; Sholl, D.S.; Jones, C.W. Modification of the Mg/DOBDC MOF with Amines to Enhance CO<sub>2</sub> Adsorption from Ultradilute Gases. *J. Phys. Chem. Lett.* **2012**, *3*, 1136–1141. [[CrossRef](#)] [[PubMed](#)]
22. Fujie, K.; Kitagawa, H. Ionic Liquid Transported into Metal–Organic Frameworks. *Coord. Chem. Rev.* **2016**, *307*, 382–390. [[CrossRef](#)]
23. Kulak, H.; Polat, H.M.; Kavak, S.; Keskin, S.; Uzun, A. Improving CO<sub>2</sub> Separation Performance of MIL-53(Al) by Incorporating 1-*n*-Butyl-3-Methylimidazolium Methyl Sulfate. *Energy Technol.* **2019**, *7*, 1900157. [[CrossRef](#)]

24. Kinik, F.P.; Altintas, C.; Balci, V.; Koyuturk, B.; Uzun, A.; Keskin, S. [BMIM][PF6] Incorporation Doubles CO<sub>2</sub> Selectivity of ZIF-8: Elucidation of Interactions and Their Consequences on Performance. *ACS Appl. Mater. Interfaces* **2016**, *8*, 30992–31005. [[CrossRef](#)] [[PubMed](#)]
25. Koyuturk, B.; Altintas, C.; Kinik, F.P.; Keskin, S.; Uzun, A. Improving Gas Separation Performance of ZIF-8 by [BMIM][BF4] Incorporation: Interactions and Their Consequences on Performance. *J. Phys. Chem. C* **2017**, *121*, 10370–10381. [[CrossRef](#)]
26. Bates, E.D.; Mayton, R.D.; Ntai, I.; Davis, J.H. CO<sub>2</sub> Capture by a Task-Specific Ionic Liquid. *J. Am. Chem. Soc.* **2002**, *124*, 926–927. [[CrossRef](#)]
27. Fukumoto, K.; Yoshizawa, M.; Ohno, H. Room Temperature Ionic Liquids from 20 Natural Amino Acids. *J. Am. Chem. Soc.* **2005**, *127*, 2398–2399. [[CrossRef](#)]
28. Sistla, Y.S.; Khanna, A. CO<sub>2</sub> Absorption Studies in Amino Acid-Anion Based Ionic Liquids. *Chem. Eng. J.* **2015**, *273*, 268–276. [[CrossRef](#)]
29. Muhammad, N.; Man, Z.B.; Bustam, M.A.; Mutalib, M.I.A.; Wilfred, C.D.; Rafiq, S. Synthesis and Thermophysical Properties of Low Viscosity Amino Acid-Based Ionic Liquids. *J. Chem. Eng. Data* **2011**, *56*, 3157–3162. [[CrossRef](#)]
30. Zhang, J.; Zhang, S.; Dong, K.; Zhang, Y.; Shen, Y.; Lv, X. Supported Adsorption of CO<sub>2</sub> by Tetrabutylphosphonium Amino Acid Ionic Liquids. *Chem.-A Eur. J.* **2006**, *12*, 4021–4026. [[CrossRef](#)]
31. Wang, X.; Akhmedov, N.G.; Duan, Y.; Luebke, D.; Hopkinson, D.; Li, B. Amino Acid-Functionalized Ionic Liquid Solid Sorbents for Post-Combustion Carbon Capture. *ACS Appl. Mater. Interfaces* **2013**, *5*, 8670–8677. [[CrossRef](#)] [[PubMed](#)]
32. Uehara, Y.; Karami, D.; Mahinpey, N. CO<sub>2</sub> Adsorption Using Amino Acid Ionic Liquid-Impregnated Mesoporous Silica Sorbents with Different Textural Properties. *Microporous Mesoporous Mater.* **2019**, *278*, 378–386. [[CrossRef](#)]
33. Uehara, Y.; Karami, D.; Mahinpey, N. Amino Acid Ionic Liquid-Modified Mesoporous Silica Sorbents with Remaining Surfactant for CO<sub>2</sub> Capture. *Adsorption* **2019**, *1*, 703–716. [[CrossRef](#)]
34. Philip, F.A.; Henni, A. Enhancement of Post-Combustion CO<sub>2</sub> Capture Capacity by Incorporation of Task-Specific Ionic Liquid into ZIF-8. *Microporous Mesoporous Mater.* **2021**, *111580*, 111580. [[CrossRef](#)]
35. Furukawa, H.; Miller, M.A.; Yaghi, O.M. Independent Verification of the Saturation Hydrogen Uptake in MOF-177 and Establishment of a Benchmark for Hydrogen Adsorption in Metal–Organic Frameworks. *J. Mater. Chem.* **2007**, *17*, 3197–3204. [[CrossRef](#)]
36. Mohamedali, M.; Henni, A.; Ibrahim, H. Investigation of CO<sub>2</sub> Capture Using Acetate-Based Ionic Liquids Incorporated into Exceptionally Porous Metal–Organic Frameworks. *Adsorption* **2019**, *25*, 675–692. [[CrossRef](#)]
37. Saha, D.; Deng, S. Structural Stability of Metal Organic Framework MOF-177. *J. Phys. Chem. Lett.* **2010**, *1*, 73–78. [[CrossRef](#)]
38. Li, Y.; Yang, R.T. Gas Adsorption and Storage in Metal–Organic Framework MOF-177. *Langmuir* **2007**, *23*, 12937–12944. [[CrossRef](#)]
39. Santos, K.M.C.; Santos, R.J.O.; De Araújo Alves, M.M.; De Conto, J.F.; Borges, G.R.; Dariva, C.; Egues, S.M.; Santana, C.C.; Franceschi, E. Effect of High Pressure CO<sub>2</sub> Sorption on the Stability of Metalorganic Framework MOF-177 at Different Temperatures. *J. Solid State Chem.* **2019**, *269*, 320–327. [[CrossRef](#)]
40. Zhu, J.; Wu, L.; Bu, Z.; Jie, S.; Li, B.G. Polyethyleneimine-Modified UiO-66-NH<sub>2</sub> (Zr) Metal–Organic Frameworks: Preparation and Enhanced CO<sub>2</sub> Selective Adsorption. *ACS Omega* **2019**, *4*, 3188–3197. [[CrossRef](#)]
41. Gaikwad, S.; Kim, Y.; Gaikwad, R.; Han, S. Enhanced CO<sub>2</sub> Capture Capacity of Amine-Functionalized MOF-177 Metal Organic Framework. *J. Environ. Chem. Eng.* **2021**, *9*, 105523. [[CrossRef](#)]
42. Aarti; Bhadauria, S.; Nanoti, A.; Dasgupta, S.; Divekar, S.; Gupta, P.; Chauhan, R. [Cu<sub>3</sub>(BTC)<sub>2</sub>]-Polyethyleneimine: An Efficient MOF Composite for Effective CO<sub>2</sub> Separation. *RSC Adv.* **2016**, *6*, 93003–93009. [[CrossRef](#)]
43. Lin, Y.; Lin, H.; Wang, H.; Suo, Y.; Li, B.; Kong, C.; Chen, L. Enhanced Selective CO<sub>2</sub> Adsorption on Polyamine/MIL-101(Cr) Composites. *J. Mater. Chem. A* **2014**, *2*, 14658–14665. [[CrossRef](#)]
44. Thi Le, M.U.; Lee, S.Y.; Park, S.J. Preparation and Characterization of PEI-Loaded MCM-41 for CO<sub>2</sub> Capture. *Int. J. Hydrog. Energy* **2014**, *39*, 12340–12346. [[CrossRef](#)]
45. Saha, D.; Wei, Z.; Deng, S. Equilibrium, Kinetics and Enthalpy of Hydrogen Adsorption in MOF-177. *Int. J. Hydrog. Energy* **2008**, *33*, 7479–7488. [[CrossRef](#)]
46. Ren, J.; Wu, L.; Li, B.G. Preparation and CO<sub>2</sub> Sorption/Desorption of N-(3-Aminopropyl)Aminoethyl Tributylphosphonium Amino Acid Salt Ionic Liquids Supported into Porous Silica Particles. *Ind. Eng. Chem. Res.* **2012**, *51*, 7901–7909. [[CrossRef](#)]
47. Gurkan, B.E.; De La Fuente, J.C.; Mindrup, E.M.; Ficke, L.E.; Goodrich, B.F.; Price, E.A.; Schneider, W.F.; Brennecke, J.F. Equimolar CO<sub>2</sub> Absorption by Anion-Functionalized Ionic Liquids. *J. Am. Chem. Soc.* **2010**, *132*, 2116–2117. [[CrossRef](#)]
48. Wang, X.; Akhmedov, N.G.; Duan, Y.; Luebke, D.; Li, B. Immobilization of Amino Acid Ionic Liquids into Nanoporous Microspheres as Robust Sorbents for CO<sub>2</sub> Capture. *J. Mater. Chem. A* **2013**, *1*, 2978–2982. [[CrossRef](#)]
49. Ferreira, T.J.; Ribeiro, R.P.P.L.; Mota, J.P.B.; Rebelo, L.P.N.; Esperança, J.M.S.S.; Esteves, I.A.A.C. Ionic Liquid-Impregnated Metal–Organic Frameworks for CO<sub>2</sub>/CH<sub>4</sub> Separation. *ACS Appl. Nano Mater.* **2019**, *2*, 7933–7950. [[CrossRef](#)]
50. Mohamedali, M.; Ibrahim, H.; Henni, A. Incorporation of Acetate-Based Ionic Liquids into a Zeolitic Imidazolate Framework (ZIF-8) as Efficient Sorbents for Carbon Dioxide Capture. *Chem. Eng. J.* **2018**, *334*, 817–828. [[CrossRef](#)]

**Disclaimer/Publisher's Note:** The statements, opinions and data contained in all publications are solely those of the individual author(s) and contributor(s) and not of MDPI and/or the editor(s). MDPI and/or the editor(s) disclaim responsibility for any injury to people or property resulting from any ideas, methods, instructions or products referred to in the content.